Weierstraß-Institut
für Angewandte Analysis und Stochastik

im Forschungsverbund Berlin e.V.

Preprint ISSN 0946 – 8633

A Lagrangian Stochastic Model for the Transport in Statistically Homogeneous Porous Media

Orazgeldi Kurbanmuradov[1], Karl K. Sabelfeld[2,3], O.F. Smidts[4]

and H. Vereecken[5]

[1] Center for Phys. Math. Research
Turkmenian State University
Turkmenbashy av. 31
744000 Ashgabad, Turkmenistan

[2] Weierstrass Institute for Applied
Analysis and Stochastics
Mohrenstraße 39
D – 10117 Berlin, Germany

[3] Institute of Comput. Mathematics
and Mathematical Geophysics
Russian Academy of Sciences
Lavrentieva str., 6
630090 Novosibirsk, Russia

[4] Université Libre de Bruxelles
50 av. F.D. Roosevelt, B-1050
Brussels - Belgium

[5] Institute of Chemistry and Dynamics of the Geosphere,
ICG IV, Agrosphere, Forschungszentrum Jülich, D-52425 Jülich - Germany

No. 786

Berlin 2002

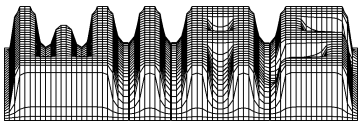

1991 *Mathematics Subject Classification.* 65C05, 76S05.

Key words and phrases. Porous media, Lognormal hydraulic conductivity, Stochastic and turbulent flows, stochastic Eulerian and Lagrangian models.

This work is supported by the Grant INTAS99-1501, and NATO Linkage Grant N 971664.

Edited by
Weierstraß-Institut für Angewandte Analysis und Stochastik (WIAS)
Mohrenstraße 39
D — 10117 Berlin
Germany

Fax: + 49 30 2044975
E-Mail: preprint@wias-berlin.de
World Wide Web: http://www.wias-berlin.de/

Abstract

A new type of stochastic simulation models is developed for solving transport problems in saturated porous media which is based on a generalized Langevin stochastic differential equation. A detailed derivation of the model is presented in the case when the hydraulic conductivity is assumed to be a random field with a lognormal distribution, being statistically isotropic in space. To construct a model consistent with this statistical information, we use the well-mixed condition which relates the structure of the Langevin equation and the probability density function of the Eulerian velocity field. Numerical simulations of various statistical characteristics like the mean displacement, the displacement covariance tensor and the Lagrangian correlation function are presented. These results are compared against the conventional random displacement method.

1 Introduction

It is well known that stochastic models are well developed for solving transport problems in turbulent flows like the transport in the atmospheric boundary layer (e.g.,see [1] - [5]). Stochastic models were constructed for a wide class of flows, in particular, to flows through porous media. (see [6, 7]). To our knowledge, in the porous media transport, only one type of stochastic models was used, namely, the Random Displacement Method (RDM) for the hydrodynamic dispersion equation. It should be stressed that RDM can be applied only if the displacement covariance tensor is known (e.g., from measurements, or numerical simulation), and cannot be applied if the functionals of interest are evaluated at times comparable with the characteristic correlation scale of the flow. In contrast, the Lagrangian stochastic models based on the tracking particles in a random velocity field extracted from numerical solution of the flow equation (for brevity, we will call this model DSM, the Direct Simulation Method) are free of these limitations, but the computational resources required are vast. Therefore, it is quite suggestive to construct a Langevin type stochastic model which is an approximation to DSM, and is written in the form of a stochastic differential equation for the position and velocity. It is worth to mention that this approach is widely used in the atmospheric transport problems. The basis for the Langevin type approach comes from the Kolmogorov similarity theory of fully developed turbulence [8] saying that the velocity structure tensor is a linear function in time which is universal in the inertial subrange. The linearity is the necessary condition to derive a Langevin type equation to mimic the behaviour of the real Lagrangian trajectories. Therefore, the crucial point of the present study is to find out if in the porous media, this kind of linear law can be observed. This problem is studied by the DSM in section 2. Detailed derivation of the Langevin type model is given in section 3. The last section deals with the numerical simulations and comparisons with the Direct Simulation Method.

2 Direct simulation method

In this section we derive Eulerian and Lagrangian statistical characteristics of the random velocity field in a porous medium. We first describe the model used to obtain the samples of the random velocity field and then analyze the properties of these random fields in the light of a Langevin type model.

2.1 Random flow model

2.1.1 Space scale

To define a random flow model in a porous medium, we need to choose first of all the space scale at which the velocity is studied. In hydrogeological literature, a distinction is made between several space scales [9, 6]. We conventionally consider (1) The microscopic scale or molecular scale where kinetics of molecules inside the pore volume is playing a role. The solid walls of the pore space may be reflecting boundaries for the molecular velocities. (2) The pore scale is the scale where the velocities are averaged over the pore volume. (3) The macroscopic (or laboratory) scale is several order of magnitude higher than the pore scale. It contains a sufficient number of pores to define the so-called "Representative Elementary Volume" (REV) where macroscopic quantity like porosity, hydraulic conductivity, etc., can be defined. In a natural formation (field), the value of a parameter over the REV is assumed pointwise. (4) The local (or formation or field) scale is the scale of a specific aquifer or field, containing one or several geological layers. (5) The regional scale may contain a system of aquifers or basins and may extend horizontally over several tens or hundreds of kilometers.

We assume in this paper that the hydrogeological properties are defined over the REV at the macroscopic scale and we derive a Langevin type model where these properties are assumed pointwise to predict transport over the field scale.

2.1.2 Darcy's law

In many general flow conditions, the phenomenological Darcy's law forms the basis of the theory of flow through porous media [6]. It is a consequence of the linearity of the equations of slow viscous flow which are obtained from the Navier-Stokes equations by neglecting the inertial terms. For time-independent flow conditions and saturated porous media, it is written as

$$\mathbf{q}(\mathbf{r}) = \theta(\mathbf{r})\,\mathbf{u}(\mathbf{r}) = -K(\mathbf{r})\,\nabla\phi(\mathbf{r}) \tag{1}$$

where $\mathbf{q}$, θ, $\mathbf{u}$, K, and ϕ are all macroscopic variables depending on space vector $\mathbf{r}$. θ is the effective (or kinematic) porosity. This porosity takes into account the volumes of voids effectively concerned with groundwater flow (that is for instance, without the dead-end pores and the adherence volume of the fluid to the grains). It is upper bounded by total porosity which is the volume occupied by the pores divided by the volume of the bulk medium. $\mathbf{q}$ is called Darcy's velocity and represents the groundwater flow rate, that is the volume of water crossing a unit area of porous medium per unit time; $\mathbf{q}$ is a measurable quantity whereas $\mathbf{u}$ is the pore velocity, that is the flow rate per unit area of fluid (which is equivalent to consider that only fluid is present). ϕ is the hydraulic potential (or pressure head). It is defined by $\phi =$

$p/\rho g + z$ where p is fluid pressure, ρ volumetric mass of the fluid, g the gravitational constant and z the height. In ϕ, the kinematic term is always neglected due to small groundwater velocities in common applications. Finally K, the proportionality coefficient between Darcy's velocity and the gradient of the hydraulic potential is called hydraulic conductivity. This parameter (and also permeability) is recognized as a key parameter for groundwater flow. Several experimental techniques (of which mainly: pumping tests, sedimentary analysis, but also seismic, geoelectrical or tracer methods) are used to intensively measure this parameter in the laboratory or in the field scale. These measurements have put in evidence the (highly) heterogeneous behaviour of K in space and have suggested the use of stochastic models.

2.1.3 Random space function

Law [10] was presumably the first who used the stochastic approach in porous media and proposed, on the basis of core analysis data from a carbonate oil field reservoir a **log-normal** probability density function (pdf) for K. Since this proposition, there is now a large body of direct evidence to support the statement that the pdf for the hydraulic conductivity is log-normal [11, 12, 6, 7]. Hydraulic log-conductivity $Y = \ln K$ is therefore commonly used and assumed to be distributed according to a Gaussian distribution $N(m_Y, \sigma_Y)$ where $m_Y =< Y >$, and σ_Y is the standard deviation.

Another parameter appearing in Eq(1) and considered in some models as a random field is the porosity θ. However its variability is recognized as much smaller than hydraulic conductivity in common applications. However a small amount of data is available for the stochastic properties of this parameter. Some linear laws, obtained on a speculative basis, have been proposed [11] to relate the porosity to log-hydraulic conductivity Y suggesting then that porosity is normally distributed.

2.1.4 The flow equation

For a time-independent problem with no water source/sink, the continuity equation may be written as

$$\nabla \mathbf{q}(\mathbf{r}) = 0 \ . \tag{2}$$

Combining this equation with Darcy's law Eq(1), we obtain the flow equation inside the flow domain $\mathcal{D}$

$$\nabla \left[K(\mathbf{r}) \, \nabla \phi(\mathbf{r}) \right] = 0 \ , \qquad \mathbf{r} \in \mathcal{D} \tag{3}$$

with the following boundary conditions over the outer surface $\mathcal{S}$

$$\begin{aligned} \phi(\mathbf{r}) &= F_D(\mathbf{r}) \ , \qquad \mathbf{r} \in \mathcal{S}_D \ , \\ \frac{\partial \phi(\mathbf{r})}{\partial n} &= F_N(\mathbf{r}) \ , \qquad \mathbf{r} \in \mathcal{S}_N \ . \end{aligned} \tag{4}$$

Here $\mathcal{S}_D$ and $\mathcal{S}_N$ are parts of $\mathcal{S}$ where the Dirichlet and Neumann boundary conditions are used, respectively. F_D and F_N are given functions over $\mathcal{S}_D$ and $\mathcal{S}_N$. The solution $\phi(\mathbf{r})$ of the flow equation (3) with the boundary conditions Eq(4) determines entirely the time-independent flow problem in a saturated porous medium because the knowledge of the hydraulic potential $\phi(\mathbf{r})$ everywhere in $\mathcal{D}$ and over $\mathcal{S}$ yields the groundwater velocity by applying Darcy's law Eq(1).

The hydraulic conductivity K in Eq(3) is considered as a random field, the hydraulic potential $\phi(\mathbf{r})$ is therefore also a random field, and the velocity is a random vector field as well. In practice, F_D and F_N are often chosen as simple deterministic functions and the boundaries are taken sufficiently far from the region of interest to avoid local effects due to the boundaries [13, 14]. Both the intensive practical measurements of the hydraulic conductivity in real applications and the central role played by this function in the flow equation Eq(3) are in favour to construct a random flow model in porous media from a random conductivity model.

Generation of the random conductivity field is followed by the solution of the flow equation (3) and by applying Darcy's law. This approach is commonly used in hydrogeology by many authors [15].

In this paper, we will focus on the following model for $Y = \ln K$:

1. Y is Gaussian with constant mean $m_Y =< Y >$ and standard deviation σ_Y.
2. Y is statistically homogeneous and isotropic with an exponential auto-correlation function
$$C_{YY}(r) = \langle Y'(\mathbf{x}+\mathbf{r})Y'(\mathbf{x})\rangle = \sigma_Y^2 \exp\left(-\frac{r}{I_Y}\right) \tag{5}$$
where I_Y is a finite and given correlation length, and $r = |\mathbf{r}|$.

2.2 Numerical simulation

The numerical calculation of several realizations of random velocity fields and the simulation of particle trajectories by the DSM follow four principal steps : (1) Generation of a hydraulic conductivity field with a prescribed statistical structure; (2) Evaluation of the Eulerian flow field by solving Eq(3) with the boundary conditions (4); (3) Identification of the particle's instantaneous position along the path line and (4) Evaluation of the statistical moments at fixed travel time or travel distance.

The accuracy of the solution depends on the numerical errors related to each step [15]. Step 1 is influenced by the choice of the generator procedure and by sampling frequency of the random field; step 2 depends on the numerical method adopted in order to solve the flow equation (3) and also on the discretization; in step 3, the error is related to the particle tracking procedure, while the convergence of step 4 depends on the dimension of the sample used in the statistical computation.

In order to limit possible inaccuracy, we considered the following numerical procedure:

1. Generation of a homogeneous random hydraulic conductivity field $K(\mathbf{r})$ in a 3D domain with the characteristics
   - $Y = \ln K$ is normal with mean $< Y >= 3.4012$ and standard deviation $\sigma_Y = 1$;
   - correlation function for log-hydraulic conductivity $C_{YY}(\mathbf{r}) =< Y'(\mathbf{x})Y'(\mathbf{x}+\mathbf{r}) >= \sigma_Y^2 \,\mathrm{Exp}(-\frac{r}{I_Y})$ where $Y' = Y - < Y >$ and $I_Y = 1$ is an isotropic correlation length;
   - the porosity $\theta(x) = \theta = 0.5$ is constant.
   - the K-field is generated by the randomized spectral formula (e.g., see [4]) with 8192 modes.

2. Solution of the groundwater flow equation for saturated conditions and time-independent problem

$$\nabla \left[K(\mathbf{r}) \nabla \phi(\mathbf{r}) \right] = 0 \tag{6}$$

and boundary condition $\phi_{y=0} - \phi(y) = J\, y$, where $J = -\nabla < \phi > \mathbf{1}_y$ is the mean hydraulic gradient. The pore velocity $\mathbf{u} = \frac{-K \nabla \phi}{\theta}$ is computed by the FORTRAN 90 code TRACE [16] which has been modified in order to write down a finite element scheme for each component of the velocity vector so that we had no need to make additional finite difference approximations when evaluating derivatives. The hydraulic potential ϕ_0 is arbitrarily chosen ($\phi_0 = 100$ m) and the mean hydraulic gradient is fixed at $\mathbf{J} = 0.01\, \mathbf{1}_y$ implying a mean groundwater velocity along the y-axis and oriented towards positive y-values. The following normalized quantities are considered

$$\widetilde{u} = \frac{u}{\frac{K_G J}{\theta}} \ , \qquad \widetilde{r} = \frac{r}{I_Y} \ , \qquad \widetilde{\phi} = \frac{\phi_0 - \phi(y)}{I_Y J} \ . \tag{7}$$

Equation (6) then becomes

$$\widetilde{\nabla} \left[e^{Y'} \widetilde{\nabla} \widetilde{\phi} \right] = 0 \tag{8}$$

with boundary conditions $\widetilde{\phi} = \widetilde{y}$. We have chosen the remaining parameters of the groundwater flow problem as follows

$$\frac{K_G J}{\theta} = 0.6 \ \rightarrow \ K_G (= e^{<Y>}) = 30, \ \text{then} \ \ < Y >= \ln 30 = 3.4012 \ .$$

The numerical values of the geometric mean $K_G = 30$ is a plausible value for hydraulic conductivity (expressed in m/day for instance) of an aquifer of moderate permeability.

3. Simulation of particle trajectories from the Eulerian velocity field.

To construct a trajectory, we solve numerically the ordinary stochastic differential equation

$$\frac{d\mathbf{X}(t)}{dt} = \mathbf{u}(\mathbf{X}(t)) \tag{9}$$

with the initial conditions: $\mathbf{X}(t_0) = \mathbf{x}_0$ and $\mathbf{u}(\mathbf{X}(t_0)) = \mathbf{u}_0$. The velocity $\mathbf{u}$ is the Eulerian velocity obtained from the flow equation. For simplicity, we used the Euler scheme

$$\mathbf{X}(t_n) = \mathbf{X}(t_{n-1}) + \mathbf{u}(\mathbf{X}(t_{n-1}))\, \Delta t \tag{10}$$

where $\Delta t = t_n - t_{n-1}$.

We define three types of domains: (a) The groundwater flow domain $\mathcal{D}$ defined in the problem (6) with deterministic boundary conditions for $y = 0$ and $y = L$. Everywhere else, a deterministic no flow boundaryïs chosen, i.e. $\nabla \phi = 0$. In our test problem, the dimensions of this domain are $[0, 50] \times [0, 70] \times [0, 50]$ corresponding to 50 times the unit correlation length I_Y perpendicular to the mean velocity and 70 times this correlation length parallel to it; (b) The flow domain $\widetilde{\mathcal{D}}$ unperturbed by deterministic boundary conditions. In hydrogeological literature [13, 14], it is well known that beyond 3 to 4 correlation lengths (or even less for impervious boundary conditions in 3D) from the deterministic boundaries the effects of these deterministic boundary conditions on the stochastic behaviour of pressure head (hydraulic potential) and therefore velocity may be neglected. We have considered here 5 correlation lengths leading to a

domain $\widetilde{\mathcal{D}}$ of dimensions : $[5,45]\times[5,65]\times[5,45]$; (c) The flow domain Ω where the particle trajectories are initiated. We have chosen empirically a domain of dimensions $[15,35]\times[15,55]\times[15,35]$. That is a domain Ω with isotropically minimum 20 correlation lengths over which a spatial mean will be sufficiently close to the ensemble mean [17].

To reproduce the stochastic behaviour of the K-field, the grid size $h_x = h_y = h_z$ is chosen in the flow problem Eq(6) to be $I_Y/4$. In practice, minimum $I_Y/3$ or $I_Y/4$ is recommended for h_x, h_y or h_z in the hydrological literature. We have then $201\times 281\times 201 = 11,352,681$ nodes in the flow problem for each realization of the random K-field. In Ω, a starting point x_0 is selected systematically at every node of the grid, that is, at $1,056,321$ nodes. It is verified that all the trajectories remain inside $\widetilde{\mathcal{D}}$. A maximum simulation time T is chosen. The time steps $\Delta t = t_n - t_{n-1}$ are variable and defined as

$$\Delta t = t_n - t_{n-1} = \text{Min}\left[T - t_{n-1}; 0.5\,\frac{\text{Min}(h_x,h_y,h_z)}{\|\mathbf{u}(t_{n-1})\|}\right] \ . \tag{11}$$

Simulation is stopped when $t_n > T$.

4. Evaluation of statistical moments at fixed travel time.

   We considered the following Lagrangian quantities: First of all, the Lagrangian correlation function for velocity. Two quantities are evaluated, the Lagrangian correlation function for the velocity component parallel to the mean flow $u_\parallel$ and the Lagrangian correlation function for the velocity component perpendicular to the mean flow $u_\perp$. They are defined by

$$C_{u_\parallel u_\parallel}(t) = \left\langle (u_\parallel(t) - < u_\parallel >)\,(u_\parallel(0) - < u_\parallel >)\right\rangle \ , \tag{12}$$

$$C_{u_\perp u_\perp}(t) = \langle (u_\perp(t) - < u_\perp >)\,(u_\perp(0) - < u_\perp >)\rangle \ . \tag{13}$$

   Then, the Lagrangian velocity structure functions: they are defined as follows:

$$< \Delta V_i(t)\,\Delta V_j(t) | X(t_0) = x_0; V(t_0) = u_0 > \ , \qquad i,j = 1,2,3 \ , \tag{14}$$

   where $\Delta V_i(t) = V_i(X(t;t_0,x_0)) - V_i(t_0)$. The quantities

$$\Delta V_i(t_n)\,\Delta V_j(t_n) \quad i,j = 1,2,3 \text{ and for} t_n \in [0,T] \tag{15}$$

   are memorized in a table according to classes for the values of $u_{0\parallel}$ and $u_{0\perp}$. Taking into account the property of homogeneity of the random K-field and thus the random Eulerian velocity field, the arithmetic mean of the quantities (15) over the number of starting points multiplied by the number of realizations of the random K-field is an approximation of the conditional means

$$< \Delta V_i(t_n)\,\Delta V_j(t_n) | V(t_0) = u_0 >$$

   regrouped in classes for the values of $u_{0\parallel}$ and $u_{0\perp}$.

   The quantities introduced above will be analysed in section 2.4 in more details. We only mention here that in order to evaluate these quantities, the time step is reduced in an appropriate way each time the simulation time is overshooting the fixed times chosen in the beginning of the simulations.

2.3 Evaluation of Eulerian characteristics

Due to the symmetry of the flow problem, the Eulerian velocity (u, v, w) is conveniently decomposed into a longitudinal velocity component $u_\parallel \equiv v$ parallel to the mean flow and a perpendicular component $u_\perp = \sqrt{u^2 + w^2}$ perpendicular to the mean flow.

We are interested in the statistical properties of the Eulerian velocity field, that is mainly, the probability density function $p_E(u, v, w)$. We decompose this pdf as follows:

$$p_E(u, v, w) = \frac{1}{2\,\pi\,u_\perp}\, p_E^{\parallel}(u_\parallel)\, p_E^C(u_\perp|u_\parallel) \tag{16}$$

where $p_E^{\parallel}(u_\parallel)$ is the marginal pdf of the Eulerian longitudinal velocity component $u_\parallel \equiv v$ and $p_E^C(u_\perp|u_\parallel)$ is the conditional pdf of the Eulerian transverse velocity component $u_\perp$ under the condition that the longitudinal component is given.

By definition we have

$$\int_{-\infty}^{+\infty} du \int_{-\infty}^{+\infty} dw\, p_E(u, v, w) = 2\,\pi \int_0^{\infty} u_\perp\, p_E\, du_\perp = p_E^{\parallel}(u_\parallel)\ . \tag{17}$$

From the numerical procedure described in section 2.2 above, we show in Fig 1 the histogram of the marginal pdf $p_E^{\parallel}(u_\parallel)$ obtained with about 1 million samples of velocities. In Fig 2, we show the histogram of the conditional pdf $p_E^C(u_\perp|u_\parallel)$ for different values of $u_\parallel$. Both figures are obtained for $\sigma_Y = 1$. Statistical calculations give $< u_\parallel >= 0.73$, $\sigma^2_{u_\parallel} = 0.33$; $< u_\perp >= 0.246$ and $\sigma^2_{u_\perp} = 0.059$. We notice that the pdf's are asymmetric with quite heavy tails. For $p_E^{\parallel}(u_\parallel)$, negative $u_\parallel$ values are possible (with very small probability) meaning counter-current velocities. For $p_E^C(u_\perp|u_\parallel)$, the shape of the pdf's highly depends on the conditional value of $u_\parallel$: the higher the value of $u_\parallel$ (in absolute value), the larger the interval of possible values for $u_\perp$.

It is well-known in the hydrogeological literature that no exact analytical expressions can be found for the pdf of the Eulerian velocity. Numerous theoretical studies [18]–[24] suggest approximations for the first and second velocity moments from Darcy's law and the flow equation by applying perturbation methods of different order in σ_Y^2. However these studies cannot describe the type of velocity pdf in general cases. These limitations can be avoided by numerical studies like in [15] where the authors thoroughly analyzed the 1st, 2nd and 3rd moments of the velocity pdf's without giving hints about a possible pdf family that could fit their numerical results.

We propose in this paper to fit the numerical pdf's with generalized Weibull distributions. We assume that for a given σ_Y,

$$p_E^C(u_\perp|u_\parallel) = \frac{p_2}{p_3^{p_1}\,\Gamma(p_1/p_2)}\,(u_\perp + p_4)^{p_1-1}\,\exp\left\{-\left[\frac{u_\perp + p_4}{p_3}\right]^{p_2}\right\}\ , \tag{18}$$

$$p_E^{\parallel}(u_\parallel) = \frac{q_2}{q_3^{q_1}\,\Gamma(q_1/q_2)}\,(u_\parallel + q_4)^{q_1-1}\,\exp\left\{-\left[\frac{u_\parallel + q_4}{q_3}\right]^{q_2}\right\}\ , \tag{19}$$

where p_3 and $q_3 > 0$; p_1, p_2, q_1 and $q_2 \geq 1$ and p_4 and $q_4 \geq 0$. p_E^C and $p_E^{\parallel}$ are generalized Weibull pdf's with shape parameters p_1 and q_1, exponents p_2 and q_2, scale parameters p_3 and q_3 and shift parameters p_4 and q_4.

It should be noted that the choice of Weibull pdf's for p_E^C and $p_E^{\|}$ is not purely arbitrary, it is indeed a quite general pdf family including the Gaussian and the Gamma pdf's. In [15], it is shown that for $\sigma_Y^2 \ll 1$ both longitudinal and transversal velocities are distributed according to a Gaussian pdf. Moreover, if the transversal components u and w are independent normally distributed with equal variances, we can show that $u_\perp = \sqrt{u^2 + w^2}$ is distributed according to the classical Weibull distribution with exponent $p_2 = 2$ and shape parameter $p_1 = p_2$.

In p_E^C, the parameters p_1 to p_4 depend on the value of the longitudinal velocity $u_\|$. The perpendicular velocity $u_\perp$ being non negative by definition, $p_4 = 0$ in Eq(18).

From Fig 2, we can intuitively suggest that $u_\|$ is playing the role of a scale parameter for the pdf p_E^C. A sensitivity analysis applied to the values of p_1, p_2 and p_3 after fitting of the numerical pdf's showed that p_3 is indeed the most sensitive parameter with respect to $u_\|$. In Fig 3, we show a law representing the dependency of p_3 with respect to $u_\|$ obtained after fitting of the pdf's p_E^C for $u_\| = -0.2$ to 2. The relation is clearly linear in $u_\|$ for $u_\| > 0$. Negative values of $u_\|$ are very improbable, and we can assume the following law for the scale parameter p_3 as a function of $u_\|$

$$p_3(u_\|) = \lambda\, u_\| + \nu \tag{20}$$

where λ, $\nu > 0$ and $\nu > \lambda\, q_4$. In Fig 3, we find, for instance, $\lambda = 0.217$ and $\nu = 0.01$.

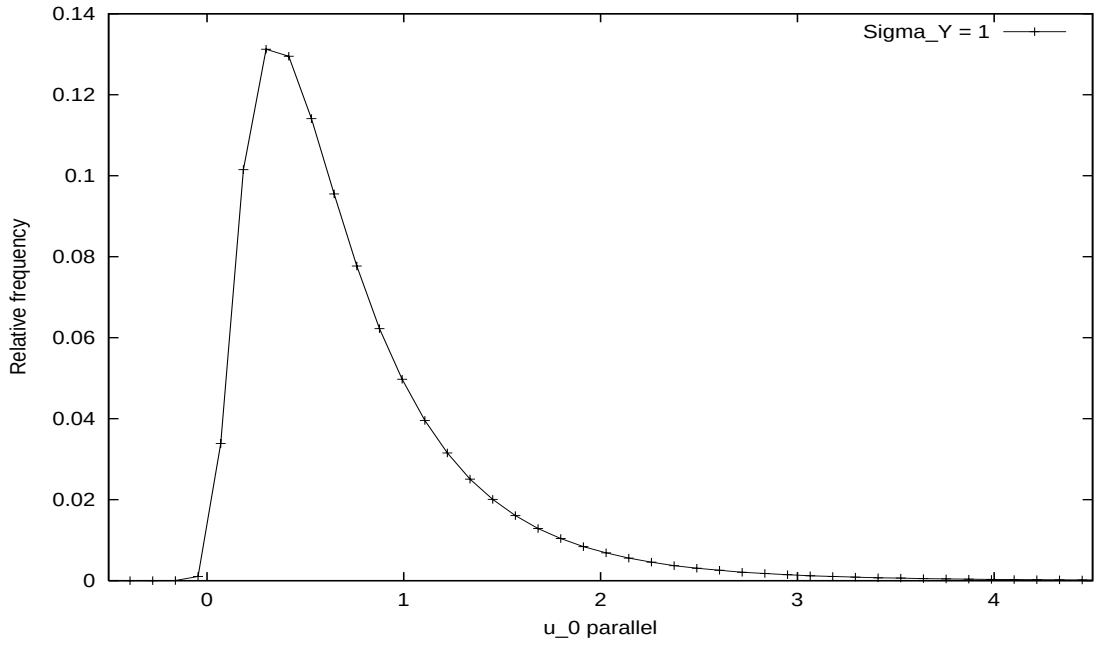

Figure 1: Histogram of the marginal pdf $p_E(u_{0\|})$.

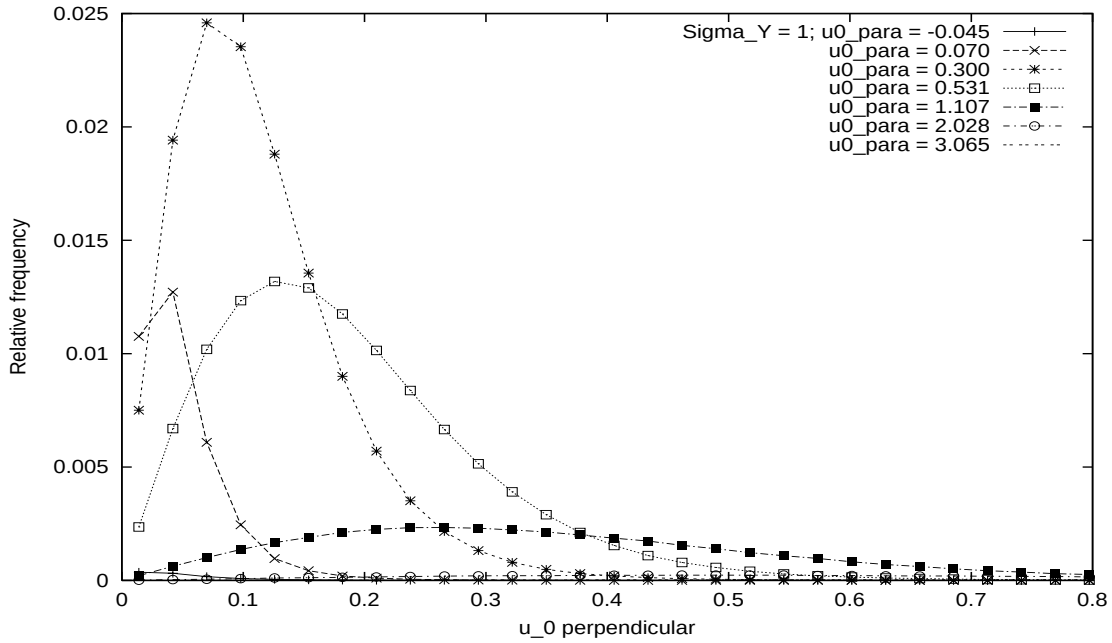

Figure 2: Histogram of the conditional pdf $p_E(u_{0\perp}|u_{0\parallel})$

2.4 Evaluation of Lagrangian characteristics

By the direct simulation method described in section 2.2, we have computed the Lagrangian correlation function $C_{u_\parallel u_\parallel}(t)$ for the component parallel to the mean flow $u_\parallel$ and the Lagrangian correlation function $C_{u_\perp u_\perp}(t)$ for the velocity component perpendicular to the mean flow $u_\perp$ defined in Eq(12) and Eq(13).

In Fig 4, the normalized correlation functions are shown versus non-dimensional time; that is $C_{u_\parallel u_\parallel}/\sigma^2_{u_\parallel}$ and $C_{u_\perp u_\perp}/\sigma^2_{u_\perp}$ versus ut/I_Y for $\sigma_Y = 1$. The results shown on this figure are similar to those obtained by Saladin and Fiorotto [15] who studied thoroughly the numerical accuracy of the DSM. From figure 4, we can obtain an estimation of the Lagrangian correlation time for the longitudinal velocity $T_L \equiv 8.2$ in units I_Y/u. It is not very sensitive to the value of σ_Y as also found in [15]. This important characteristic time determines the validity range of the approximations introduced in the random displacement model as seen in section 4.

Second quantity essential for the Langevin model developed in this paper is the velocity structure function introduced in Eq(14).

A series of calculations were realized by accumulating the results of $\Delta V_i(t_n)\Delta V_j(t_n)$ for $T = 2$, 20 time intervals, 30 classes for $u_{0\parallel}$ and 35 classes for $u_{0\perp}$. Trajectories were initiated from each node of the grid in the domain Ω, that is, at $1,056,321$ points and a number of 40 realizations of the K and velocity fields were considered (generated from TRACE using parallel-processing over 64 CPUs).

In Fig 5, the velocity structure function $< \Delta V_x(t)\, \Delta V_x(t) | \mathbf{V}(t_0) = \mathbf{u}_0 >$ is shown versus time for $0.144 < u_0 < 0.350$ where u_0 is the norm of $\mathbf{u_0}$. The error bars appearing in this and the following figures represent the 90% confidence interval of the results obtained after averaging over

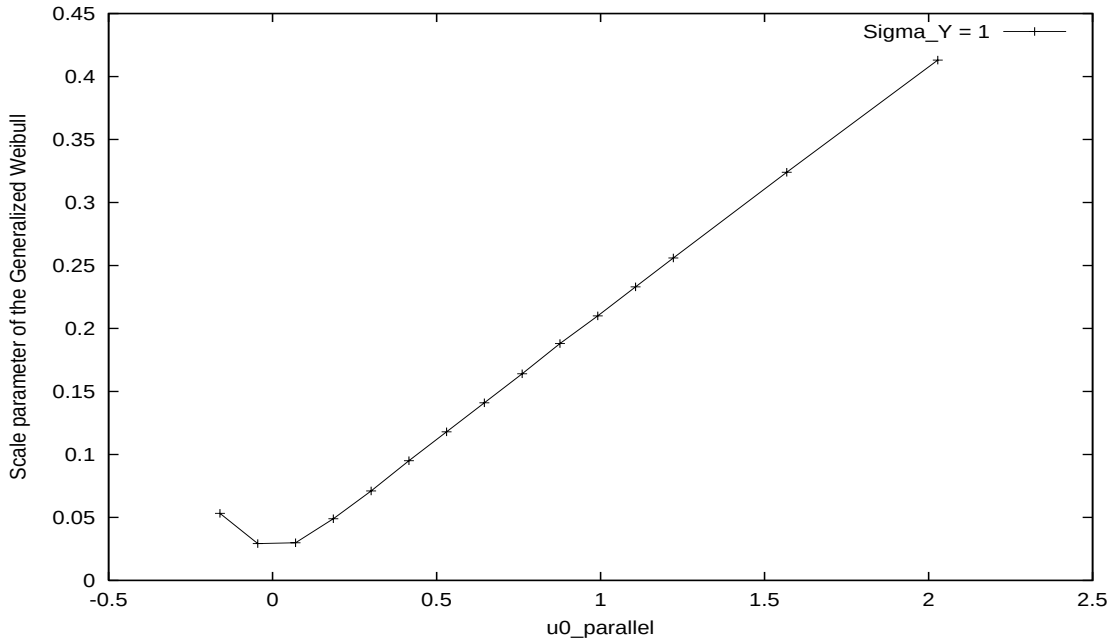

Figure 3: Dependence of the conditional pdf $p_E(u_{0\perp}|u_{0\parallel})$ on $u_{0\parallel}$.

the trajectories. It is reminded here that the x-axis is perpendicular to the mean flow. Similar results are obtained for the function $< \Delta V_z(t)\, \Delta V_z(t) | \mathbf{V}(t_0) = \mathbf{u}_0 >$ where z is the other axis perpendicular to the mean flow. The calculations show that a linear behaviour of this function versus time can be identified. This linear behaviour is appearing after a quadratic behaviour versus time. In Fig 6, the velocity structure function $< \Delta V_y(t)\, \Delta V_y(t) | \mathbf{V}(t_0) = \mathbf{u}_0 >$ is also shown versus time, for the same u_0 range. The y-axis is here parallel to the mean flow. Also in this figure a linear behaviour of the structure function can be seen after a quadratic behaviour and for the same time period. The numerical results show that the values of the velocity structure functions $< \Delta V_x(t)\, \Delta V_y(t) | \mathbf{V}(t_0) = \mathbf{u}_0 >$ and $< \Delta V_x(t)\, \Delta V_z(t) | \mathbf{V}(t_0) = \mathbf{u}_0 >$ are much smaller and no clear linear behaviour may be identified. By symmetry, similar results as $< \Delta V_x(t)\, \Delta V_y(t) | \mathbf{V}(t_0) = \mathbf{u}_0 >$ are obtained for $< \Delta V_y(t)\, \Delta V_z(t) | \mathbf{V}(t_0) = \mathbf{u}_0 >$. In Fig. 7 and 8, the velocity structure functions $< \Delta V_x(t)\, \Delta V_x(t) | \mathbf{V}(t_0) = \mathbf{u}_0 >$, $< \Delta V_y(t)\, \Delta V_y(t) | \mathbf{V}(t_0) = \mathbf{u}_0 >$ and $< \Delta V_x(t)\, \Delta V_y(t) | \mathbf{V}(t_0) = \mathbf{u}_0 >$ are also shown versus time for a higher intensity of $\mathbf{u_0}$; in this example $1.427 < u_0 < 1.629$.

From these results, we see that a linear behaviour of the velocity structure function may be identified. By considering that the groundwater velocity along the trajectory at early times is close to the value at the starting point u_0, we may deduce that between a distance along the path of about 40 to 70 % of the correlation length I_Y, the linear regime is effective. This statement was verified for many different values of the starting velocity, values of σ_Y and I_Y. For every class of velocity u_0, the tensor b with components

$$b_{ij} = \lim_{t \to \varepsilon} \frac{1}{t} \; < \Delta V_i(t)\, \Delta V_j(t) | \mathbf{X}(t_0) = \mathbf{x}_0; \mathbf{V}(t_0) = \mathbf{u}_0 > \tag{21}$$

can be computed from the linear law observed in the Lagrangian velocity structure function.

We computed the quantities b_{ij} from the different Lagrangian velocity structure functions versus time by applying the formula (21) for a time ε in the range $(0.4\,\frac{I_Y}{||u_0||}\,,\,0.7\,\frac{I_Y}{||u_0||})$. The dependency of the components b_{ij} with respect to the normalized quantities defined in Eq(7) can be written as

$$b_{ij} \equiv b_{ij}(\sigma_Y, \widetilde{u}_{0\parallel}, \widetilde{u}_{0\perp}) \ . \tag{22}$$

We show as an example in figures 9 to 12 the behaviour of b_{ij} (here b_{xx} and b_{yy}) with respect to $u_{0\parallel}$ and $u_{0\perp}$ for given values of $u_{0\perp}$ and $u_{0\parallel}$, respectively and for $\sigma_Y = 1$. The curves have been obtained by a bicubic interpolation for the variables $u_{0\parallel}$ and $u_{0\perp}$. By comparing Eulerian pdf's $p_E^{\parallel}(u_\parallel)$ and $p_E^C(u_\perp|u_\parallel)$ obtained in section 2.3, we notice that in the zone of interest (where the density is non-zero; that is typically for $u_{0\parallel} \in [0.3, 1.2]$ and for $u_{0\perp} \in [0.05, 0.45]$ in this example) the values of b_{xx} and b_{yy} are smoothly varying. A first approximate model is to assume a constant value for these quantities. This is the model we consider in this paper.

Finally, in Fig. 13, we show as an example b_{xx} w.r.t. $u_{0\parallel}$ for $\sigma_Y = 0.5$. We see clearly that the dependency of b_{ij} w.r.t. σ_Y is much stronger than the dependency w.r.t. $u_{0\parallel}$.

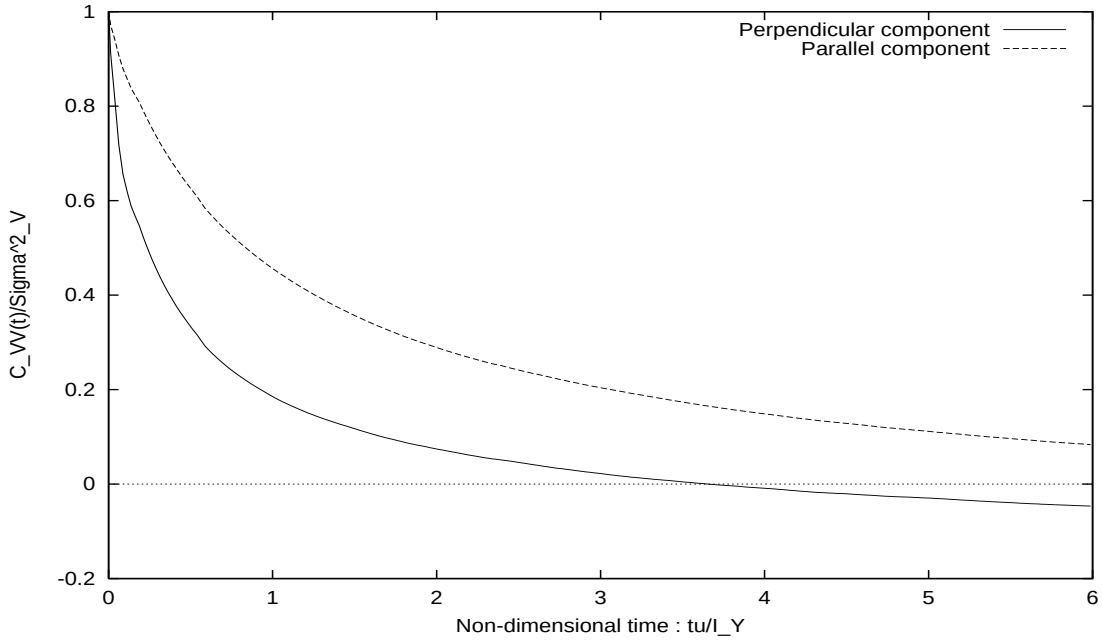

Figure 4: Lagrangian Correlation functions for parallel and perpendicular velocity components.

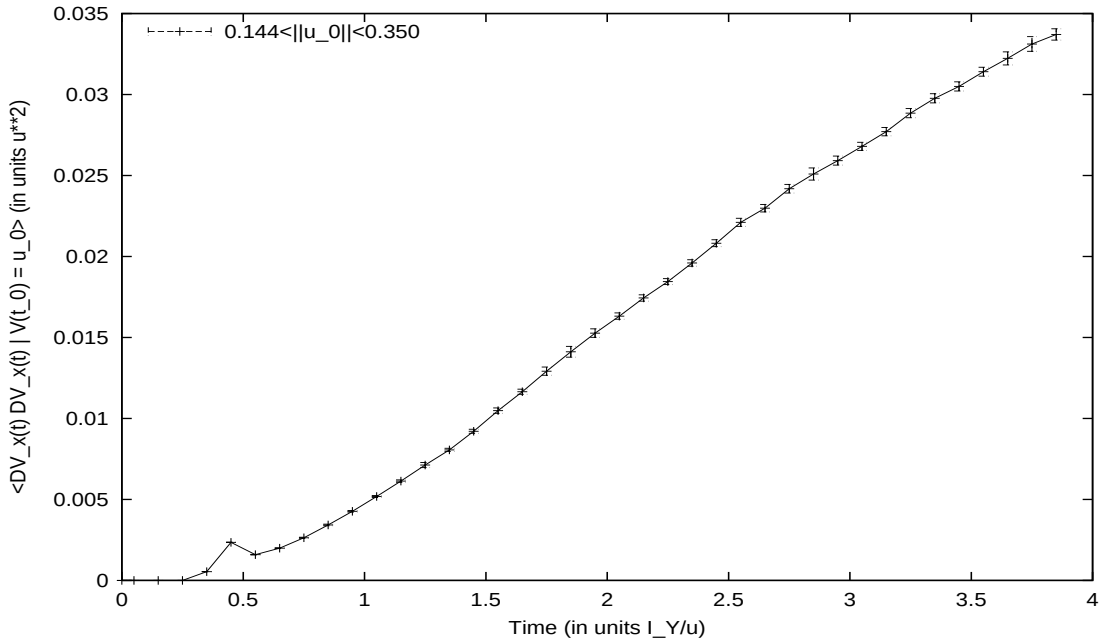

Figure 5: Velocity structure function versus time (xx component); linear regime from $t \simeq 1.3$.

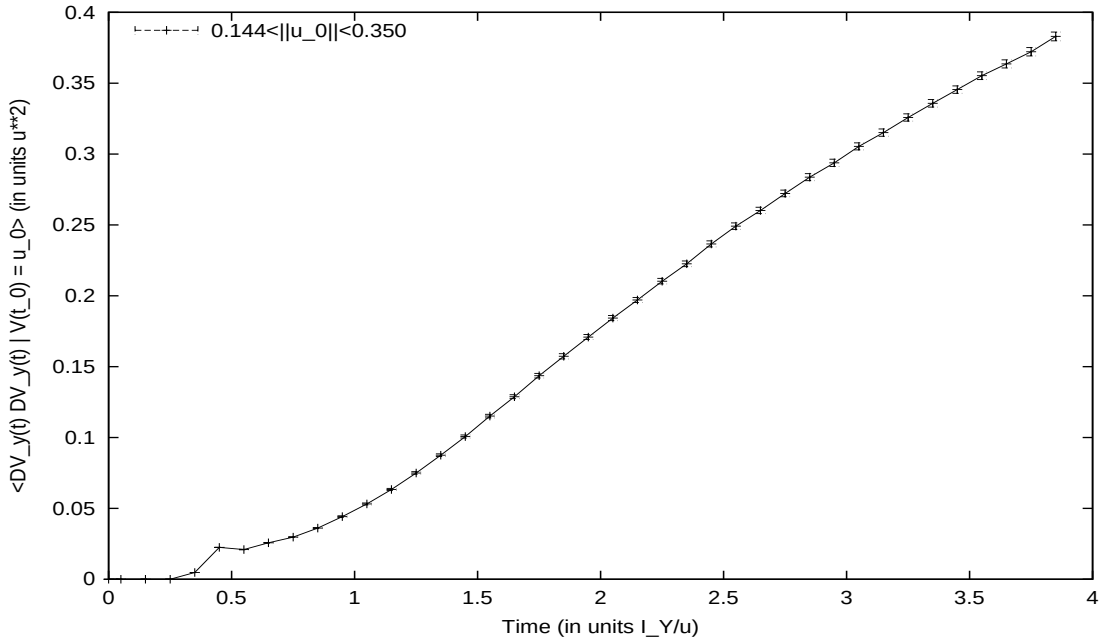

Figure 6: Velocity structure function versus time (yy component) ; linear regime from $t \simeq 1.3$.

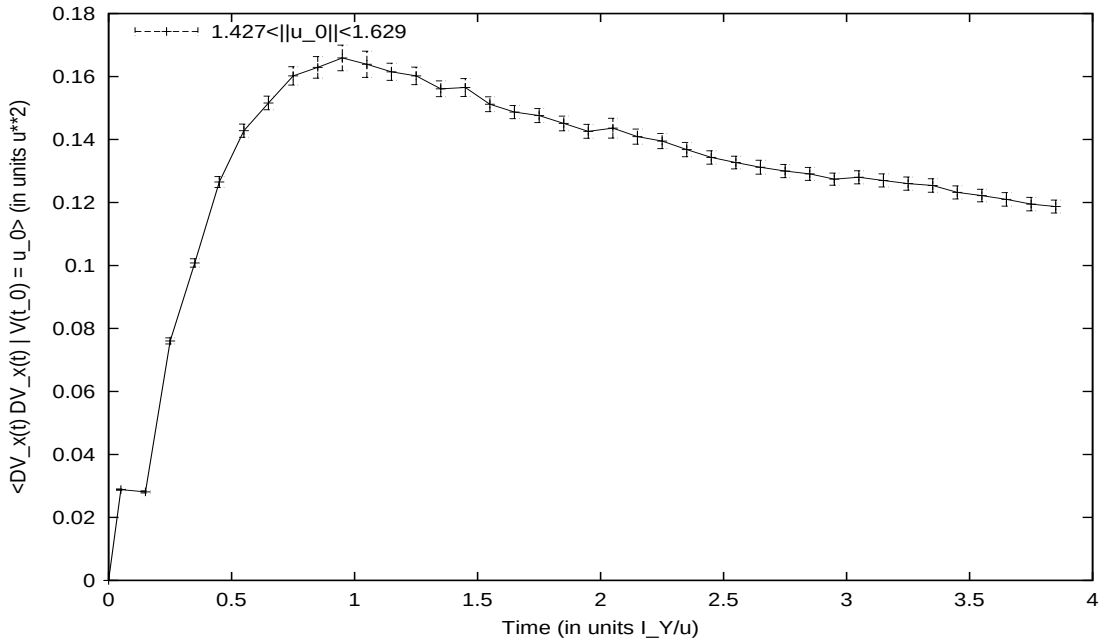

Figure 7: Velocity structure function versus time (xx component) ; linear regime for $t \in (0.4, 0.6)$.

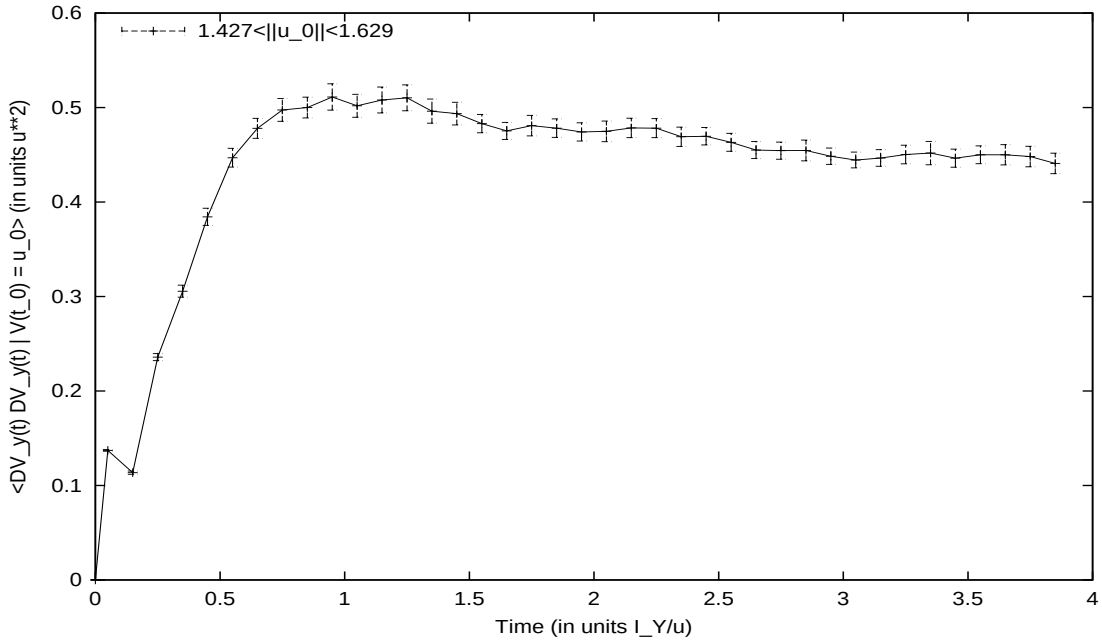

Figure 8: Velocity structure function versus time (yy component) ; linear regime for $t \in (0.4, 0.6)$.

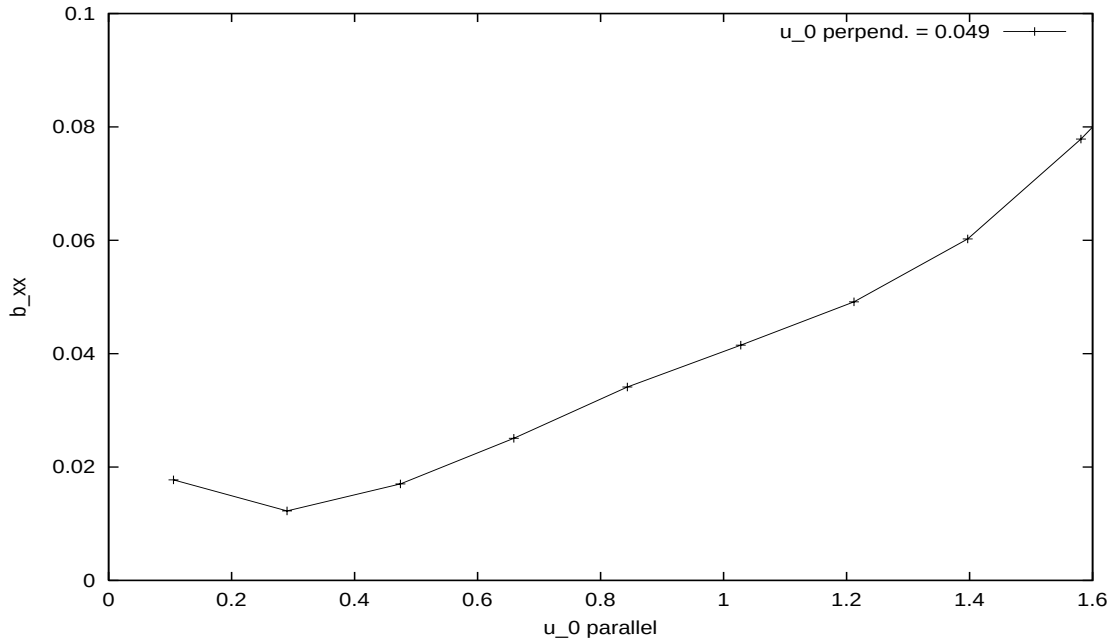

Figure 9: Bicubic interpolation for b_{xx}.

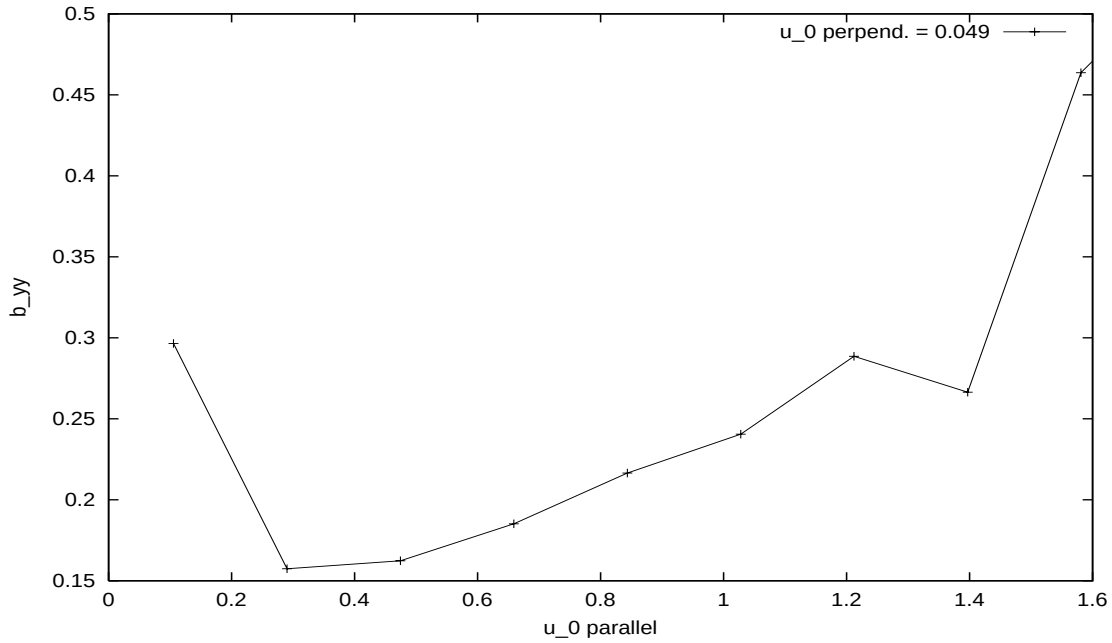

Figure 10: Bicubic interpolation for b_{yy}.

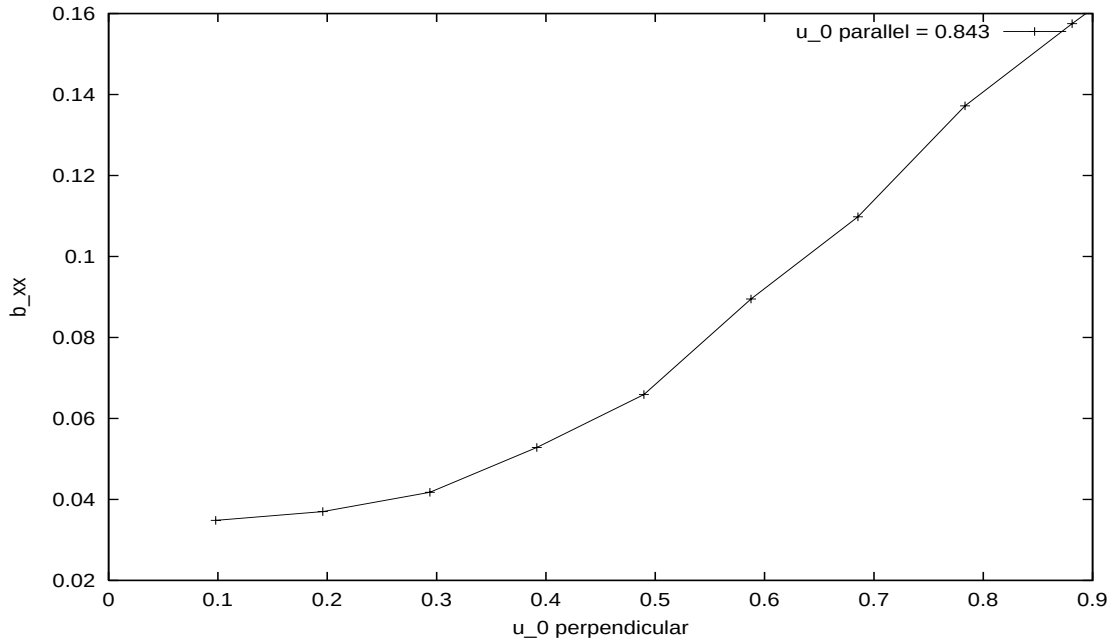

Figure 11: Bicubic interpolation for b_{xx}.

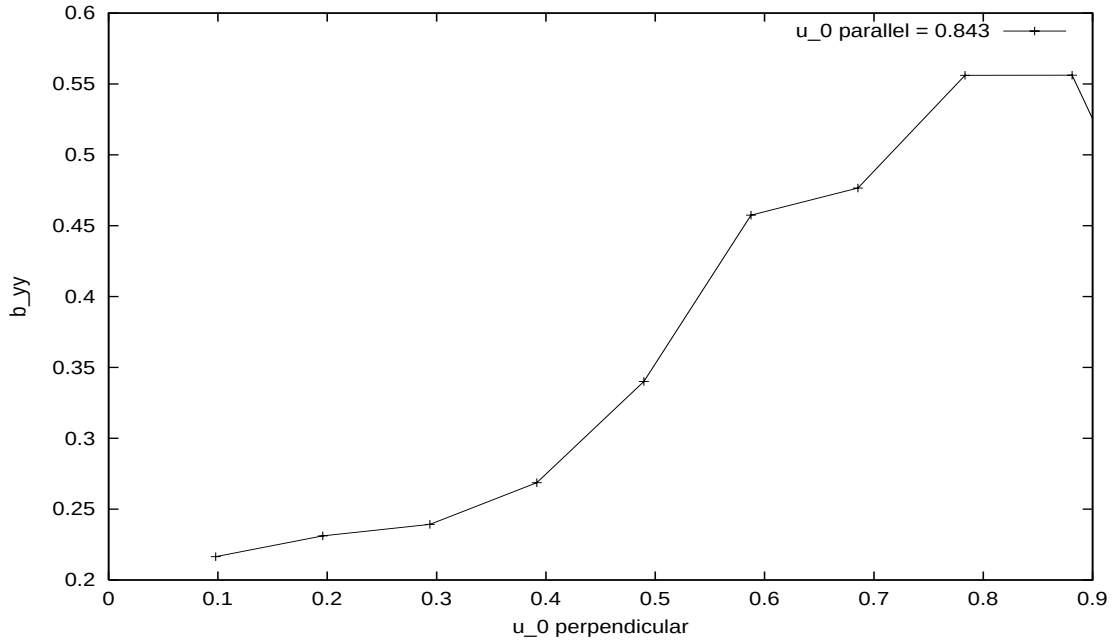

Figure 12: Bicubic interpolation for b_{yy}.

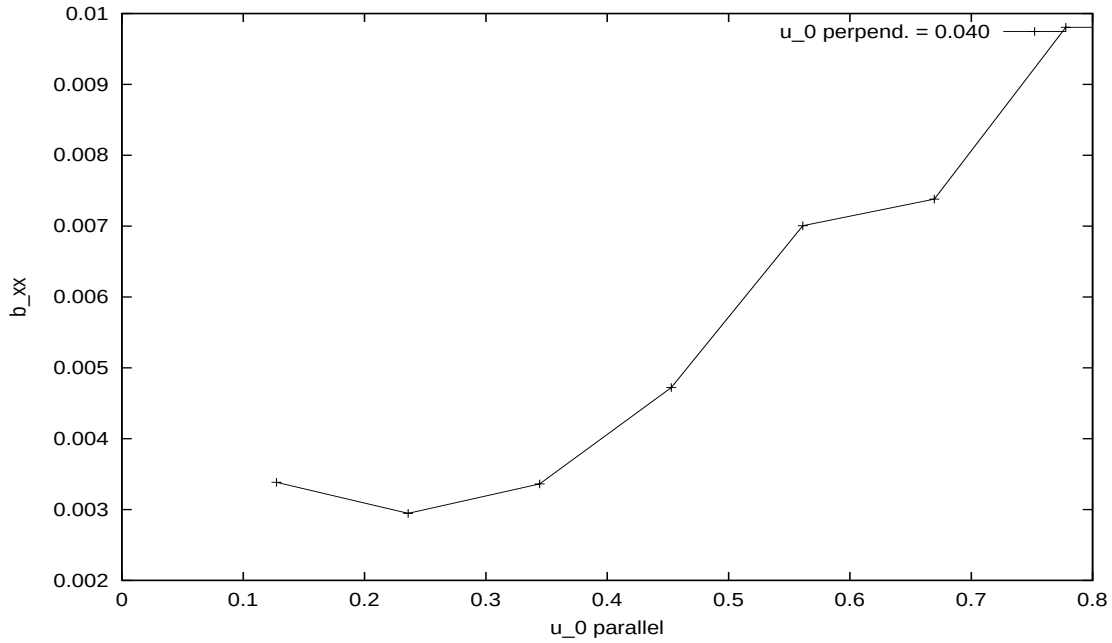

Figure 13: Bicubic interpolation for b_{xx}.

3 Construction of the Langevin type model

3.1 Introduction

The Langevin type models assume that the trajectory $(\mathbf{X}(\mathbf{t}), \mathbf{V}(\mathbf{t}))$ of a particle is governed by a stochastic differential equation of Ito type

$$\begin{aligned} dX_i(t) &= V_i\, dt, \\ dV_i(t) &= a_i(\mathbf{X}(t), \mathbf{V}(t), t)\, dt + \sigma_{ij}(\mathbf{X}(t), \mathbf{V}(t), t)\, dB_j(t), \qquad i = 1, 2, 3. \end{aligned} \tag{23}$$

The summation convention over the repeated indices is used. Here a_i are the drift, and σ_{ij} the diffusion terms, and B_j are standard independent Wiener processes.

This kind of models is widely used in atmospheric turbulence simulations (e.g., see [2], [3], [5]). The motivation comes from the fact that the characteristic time of the acceleration correlations is much less than that for the velocity correlations which is the case for the turbulent flow.

In porous medium when dealing with laminar flows we cannot treat the velocity as turbulent. However the acceleration direction is highly varying because of the pore structure inhomogeneity. Therefore, the acceleration and velocity fields can be considered as random flows, and the Langevin type equations can be used to describe the Lagrangian dynamics as in Eq(24). The main difference, compared to the turbulence, is that the flow in porous media is extremely anisotropic, which results in much more complicated form of the drift and diffusion terms. In particular, here we do not have this nice and simple diffusion term in the form of a constant C_0 coming from the Kolmogorov theory (e.g., see [1]).

Compared to RDM models, the Langevin type models involve more information about the statistics of velocity, e.g., it naturally uses the information about the pdf of the Eulerian velocity field. Indeed, in case the velocity is incompressible, it is known that the Eulerian pdf p_E is related to the coefficients of the Langevin equation Eq(24) through the well-mixed condition [2]:

$$\frac{\partial p_E}{\partial t} + u_i \frac{\partial p_E}{\partial x_i} + \frac{\partial}{\partial u_i}(a_i p_E) = \frac{1}{2}\frac{\partial^2 (b_{ij}\, p_E)}{\partial u_i \partial u_j} \tag{24}$$

where $b_{ij} = \sigma_{ik}\sigma_{jk}$.

This complicates the model, but wins very important gains: the model is able to describe the transport in details for scales inside or compared to the Lagrangian time scale where the dispersion is not linear, so generally we deal here with the super-diffusion. For instance, it is possible to evaluate the concentration field not far from the source. Thus, these models are free of the Fickian hypothesis.

Derivation of the drift and diffusion terms is not simple. So far, even in the well studied atmospheric turbulence, there is no theoretical approach which derives uniquely the expressions for these terms. Therefore, experimental and heuristical information is used to determine the model. In our case we evaluated the diffusion term from numerical solution of the flow equations reported in the previous section. In the next section, we derive the drift term from the well-mixed condition Eq(24).

3.2 Langevin model for isotropic porous medium

We derive our Langevin model for a porous medium in which the flow conditions and properties of the random hydraulic conductivity field are similar to those described in section 2, that is, the mean horizontal flow is uniform over the domain $\mathcal{D}$, and it is assumed that the hydraulic conductivity field is log-normally distributed, with isotropic exponential correlation function.

To derive a unique Langevin model with these types of flow conditions we make the following general assumptions :

Let us construct the drift coefficients $a_1 = a_u$, $a_2 = a_v$, and $a_3 = a_w$ in the following general form

$$a_u = \frac{1}{2p_E}\frac{\partial}{\partial u}(b_u^2 p_E) + \frac{u\phi}{p_E}\ , \quad a_v = \frac{1}{2p_E}\frac{\partial}{\partial v}(b_v^2 p_E) + \frac{\psi}{p_E}\ , \quad a_w = \frac{1}{2p_E}\frac{\partial}{\partial w}(b_w^2 p_E) + \frac{w\phi}{p_E}\ ,$$

where the functions $\phi = \phi(u_\perp, v)$ and $\psi = \psi(u_\perp, v)$ should satisfy the equation (actually, the well-mixed condition):

$$\frac{\partial(u\phi)}{\partial u} + \frac{\partial \psi}{\partial v} + \frac{\partial(w\phi)}{\partial w} = 0\ .$$

The crucial point of the model is now the following: we introduce the characteristic time scale of the transverse velocity τ_p as follows: $\tau_p = \frac{\alpha I_Y}{\bar{U}}$ where $\bar{U}$ is the mean longitudinal velocity ($\bar{U} =< u_\parallel >$), I_Y is the correlation length of the log hydraulic conductivity (in our case $I_Y = 1$, $\bar{U} = 0.73$), and α is a dimensionless constant.

This is the simplest choice motivated by dimensional arguments. Note that the dimension of ϕ/p_E is $[time^{-1}]$, so we simply suggest that

$$\frac{\phi}{p_E} = -\frac{1}{\tau_p}. \tag{25}$$

Hence we have $\phi = -G\,p_E$ where we define the constant

$$G = \bar{U}/(\alpha I_Y). \tag{26}$$

We can then rewrite the well-mixed condition in the form:

$$\frac{\partial \phi}{\partial u_\perp}\frac{u^2+w^2}{u_\perp} + 2\phi + \frac{\partial \psi}{\partial v} = 0,$$

i.e.,

$$\frac{\partial \psi}{\partial v} = G p_E[2 + u_\perp \frac{\partial \ln p_E}{\partial u_\perp}].$$

From this, we find $\psi(u_\perp, v)$ by choosing $\psi(u_\perp, \infty) = 0$:

$$\psi(u_\perp, v) = -\int_v^\infty G p_E(u_\perp, v')[2 + u_\perp \frac{\partial \ln p_E}{\partial u_\perp}]\, dv'. \tag{27}$$

Thus the coefficients a_u, a_v, a_w are defined, and our model includes one free parameter α.

Let us now describe the numerical implementation. We have to solve the system:

$$dX = u\,dt, \quad dY = v\,dt, \quad dZ = w\,dt, \tag{28}$$

$$\begin{aligned} du &= a_u\,dt + b_u\,dB_u(t), \\ dv &= a_v\,dt + b_v\,dB_v(t), \\ dw &= a_w\,dt + b_w\,dB_w(t). \end{aligned} \tag{29}$$

Note that we can write

$$\begin{aligned} a_u &= u\,g(u_\perp, v), \\ a_v &= h(u_\perp, v), \\ a_w &= w\,g(u_\perp, v) \end{aligned} \tag{30}$$

where

$$g(u_\perp, v) = -G + \frac{1}{2u_\perp}\frac{\partial b_u^2}{\partial u_\perp} + \frac{b_u^2}{2u_\perp}\frac{\partial \ln p_E}{\partial u_\perp} \ , \tag{31}$$

$$\begin{aligned} h(u_\perp, v) &= \frac{1}{2}\frac{\partial b_v^2}{\partial v} + \frac{1}{2}\, b_v^2\, \frac{\partial \ln\, p_E}{\partial v} \\ &\quad -\frac{1}{p_E}\int_v^\infty G\, p_E(u_\perp, v')\, \left[2 + u_\perp\, \frac{\partial \ln p_E(u_\perp, v')}{\partial u_\perp}\right] dv' \end{aligned} \tag{32}$$

and where the diffusion coefficients b_u^2, b_v^2 and b_w^2 are known from section 2.4.

3.3 Expressions of the drift terms

We have seen in section 2.3 that the pdf's of the Eulerian velocity may be fitted by the following Weibull densities :

$$p_E^C(u_\perp|u_\parallel) = \frac{p_2}{p_3(u_\parallel)^{p_1}\,\Gamma(p_1/p_2)}\, u_\perp^{p_1-1}\, \exp\left\{-\left[\frac{u_\perp}{p_3(u_\parallel)}\right]^{p_2}\right\} \ , \tag{33}$$

$$p_E^\parallel(u_\parallel) = \frac{q_2}{q_3^{q_1}\,\Gamma(q_1/q_2)}\, (u_\parallel + q_4)^{q_1-1}\, \exp\left\{-\left[\frac{u_\parallel + q_4}{q_3}\right]^{q_2}\right\} \ . \tag{34}$$

We have also seen that the dependence of p_E^C on $u_\parallel$ may be restricted to the scale parameter p_3 only, which depends linearly on $u_\parallel$ (see the relation (20)). Finally, from the Lagrangian characteristics studied in section 2.4, we may model, as a first approximation, the diffusion coefficients by the following simple laws:

$$b_u^2 = b_1 + c_1\, u_\perp \ , \qquad b_v^2 = b_2 + c_2\, u_\perp \ , \qquad b_w^2 = b_u^2 \tag{35}$$

where b_1, b_2, c_1 and c_2 are constants.

From Eq(30) and (32) and using the expressions (33) and (34) for p_E and (35) for b_v^2, we obtain for the longitudinal drift term $a_\parallel$

$$\begin{aligned} a_\parallel &= \frac{1}{2}\, b_\parallel^2 \left\{\frac{1}{u_\parallel + q_4}\, \left[q_1 - 1 - q_2\, \left(\frac{u_\parallel + q_4}{q_3}\right)^{q_2}\right]\right. \\ &\quad \left. + \frac{1}{u_\parallel + \frac{\nu}{\lambda}}\, \left[p_2 \left(\frac{u_\perp}{\lambda\, u_\parallel + \nu}\right)^{p_2} - p_1\right]\right\} \\ &\quad -\frac{G}{p_E(u_\perp, u_\parallel)} \int_{u_\parallel}^{\infty} p_E(u_\perp, u'_\parallel)\, [\, p_1 - p_2 \left(\frac{u_\perp}{\lambda u'_\parallel + \nu}\right)^{p_2}\,]\, du'_\parallel \ . \end{aligned} \tag{36}$$

Similarly, using again the expressions (33) and (34) for p_E and (35) for b_u^2 and b_w^2, we obtain for the transverse drift components from (30) and (31)

$$a_u = u\, g(u_\perp, u_\parallel), \quad a_w = w\, g(u_\perp, u_\parallel)$$

where the friction function g is given by

$$g(u_\perp, u_\parallel) = -G + \frac{1}{2}\left\{\frac{c_1}{u_\perp} + \frac{b_\perp^2}{u_\perp^2}\left[p_1 - 2 - p_2\left(\frac{u_\perp}{\lambda\, u_\parallel + \nu}\right)^{p_2}\right]\right\} . \tag{37}$$

In the expressions (36) and (37) found above for the longitudinal drift term and the transverse friction function, we may find the following physical interpretations :

1. When $u_\parallel$ decreases to small values (close to $-q_4$), $a_\parallel$ becomes large and positive whereas when $u_\parallel \gg q_4$, $a_\parallel$ becomes large in absolute value and negative. This behaviour of the acceleration $a_\parallel$ with respect to $u_\parallel$ at the boundaries is expected to avoid divergence of the longitudinal velocity values towards large negative or positive values in the simulation of the Langevin model.

2. We see that g is large and positive for $u_\perp \to 0$, whereas g is large in absolute value and negative when $u_\perp \to \infty$ and $u_\parallel \to -q_4$. This behaviour of g with respect to $u_\perp$ at the boundaries is expected to avoid divergence of the transverse velocity values towards zero or large positive values.

To make the simulations efficient we make the tabulation of the functions $g(u_\perp, u_\parallel)$ and $h(u_\perp, u_\parallel)$ in the domain K:

$$K = [\,(u_\perp, u_\parallel) : \quad u_{\parallel\,\min} \le u_\parallel \le u_{\parallel\,\max}, 0 \le u_\perp \le C_u\, u_\parallel],$$

where C_u is a constant, and $u_{\parallel\,\min}$ and $u_{\parallel\,\max}$ are the limits chosen so that the simulation gives stable results.

4 Numerical results and comparison against the DSM

It is important to verify that the new Langevin model developed in this paper is able to reproduce the behaviour of some major characteristics of the transport of contaminants in porous media. We have therefore fitted the parameters of the Langevin model introduced in section 3.2 to the dispersion curves versus time. Figures 14 and 15 present the trajectories simulated by DSM and Langevin model, respectively. The Langevin model derived from the equations (29), (30) to (32) mimic the real Lagrangian trajectories given by the Direct Simulation Method. Even if we see clearly that the structure of trajectories is quite different, the fact that the well-mixed condition is satisfied guarantees the correct consistency of the simulation results with the Eulerian pdf which in turn assures that the mean concentrations should be close. By fixing the free parameter α appearing in the definition of the constant G in (26)), it is possible to fit the Langevin model to some fundamental transport characteristics as transverse and longitudinal dispersion versus time. By using the results of section 2.4, we identified the coefficients of the simple linear laws (35) modelling, as a first approximation, the diffusion coefficients $b_\parallel^2$ and $b_\perp^2$.

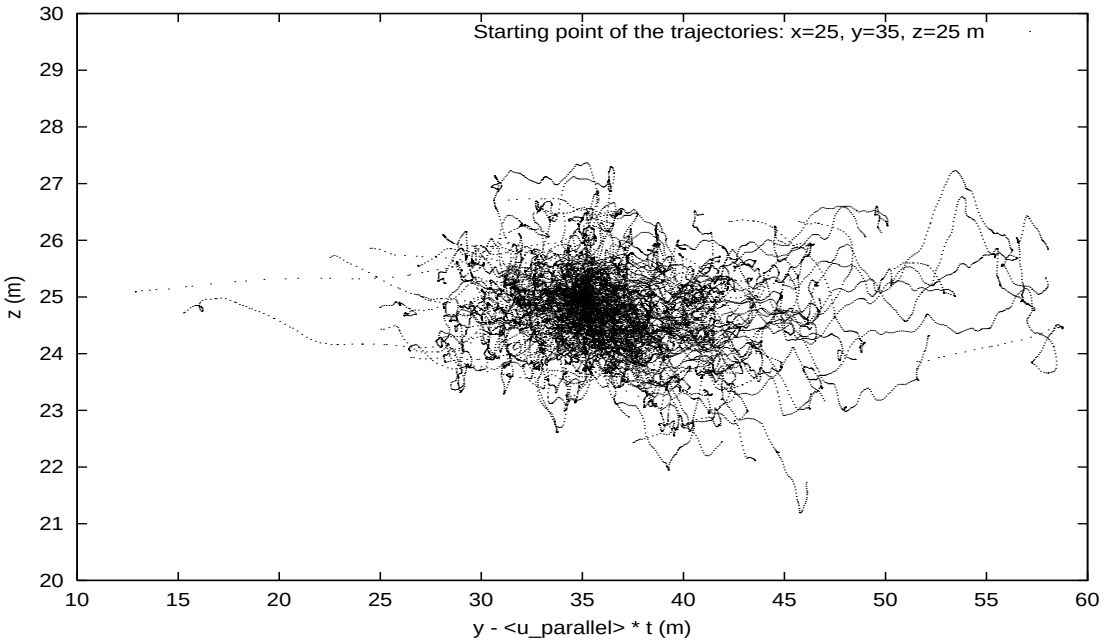

Figure 14: View of 500 DSM trajectories during 5 Lagrangian correlation time.

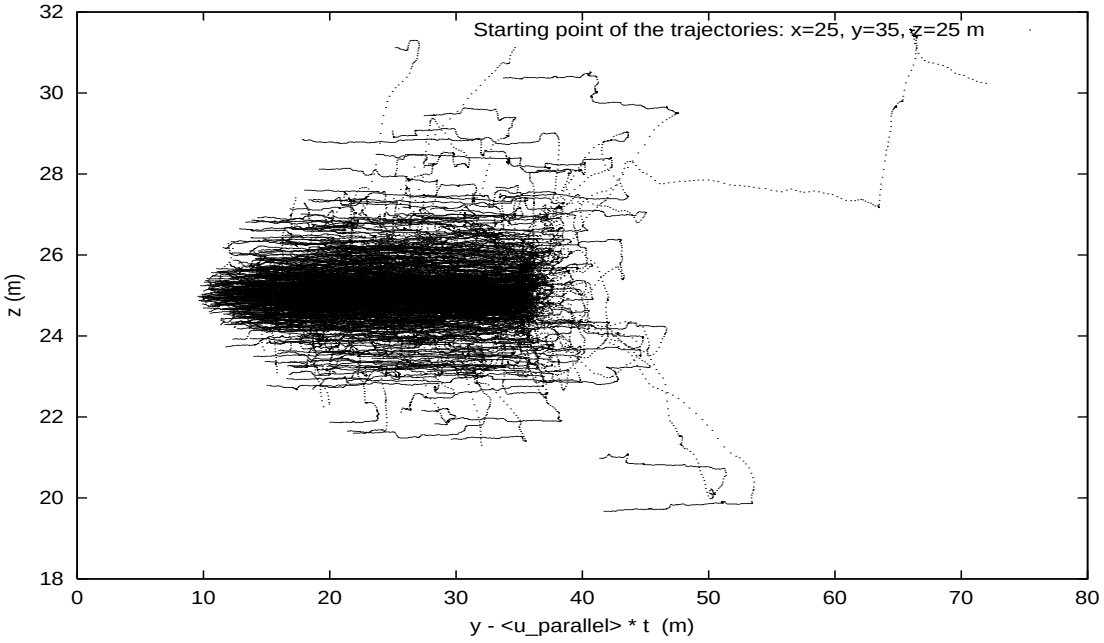

Figure 15: View of 500 Langevin trajectories during 5 Lagrangian correlation time.

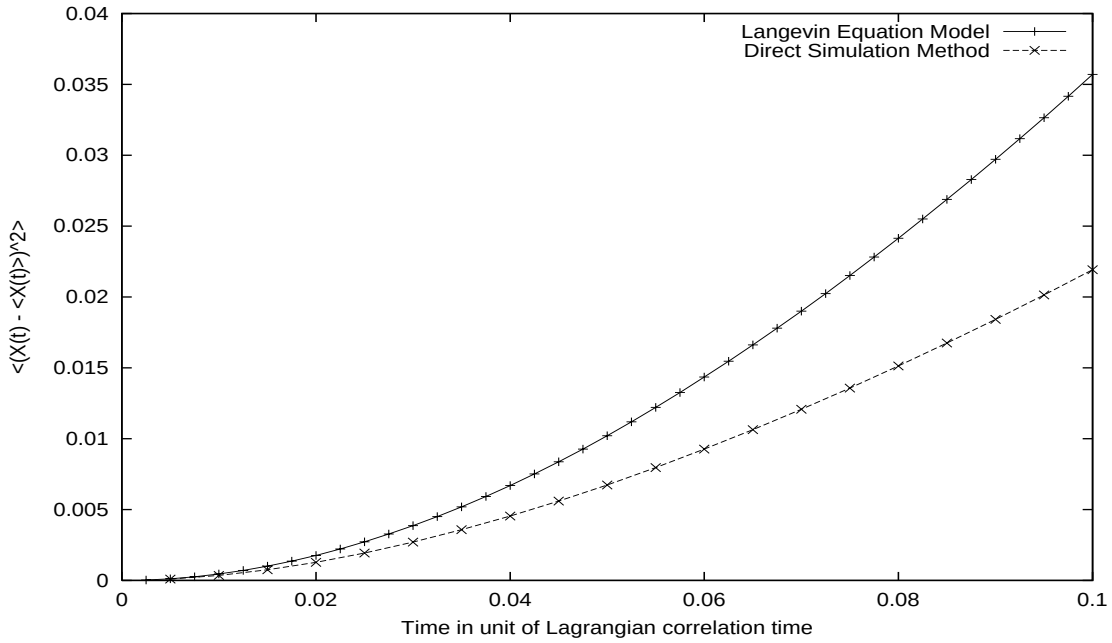

Figure 16: Comparison between Langevin model and DSM of the transverse dispersion component for small times.

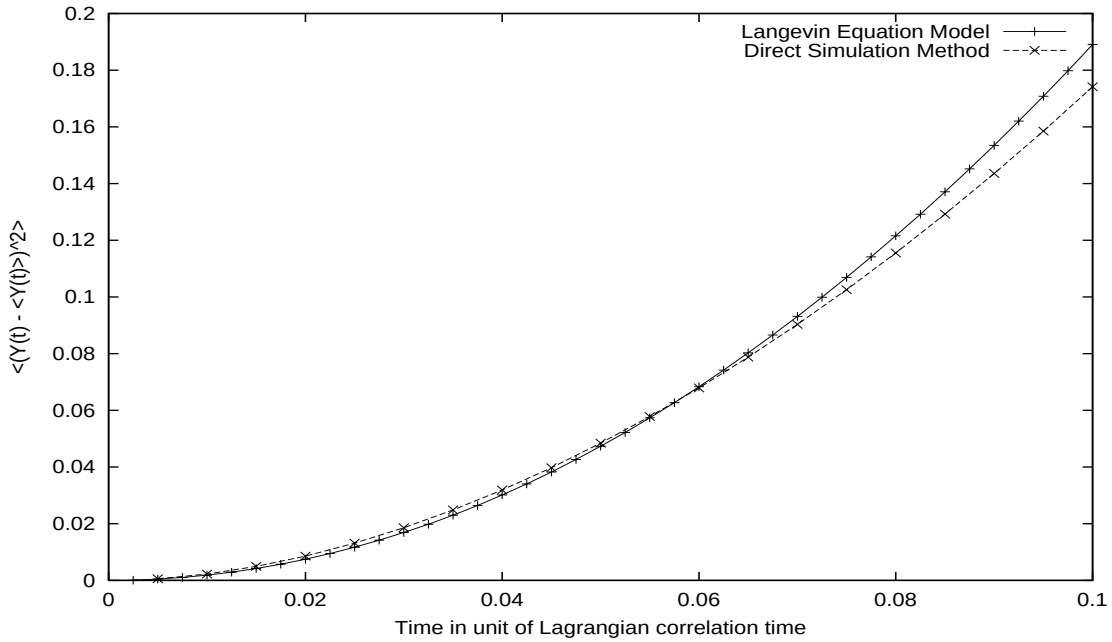

Figure 17: Comparison between Langevin model and DSM of the longitudinal dispersion component for small times.

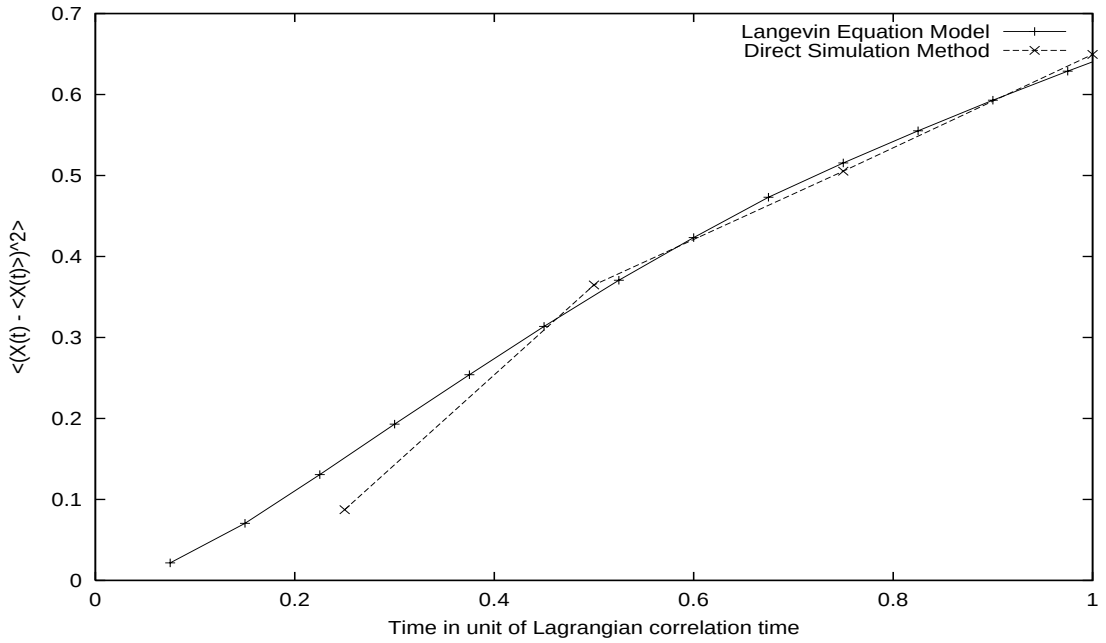

Figure 18: Comparison between Langevin model and DSM of the transverse dispersion component for large times.

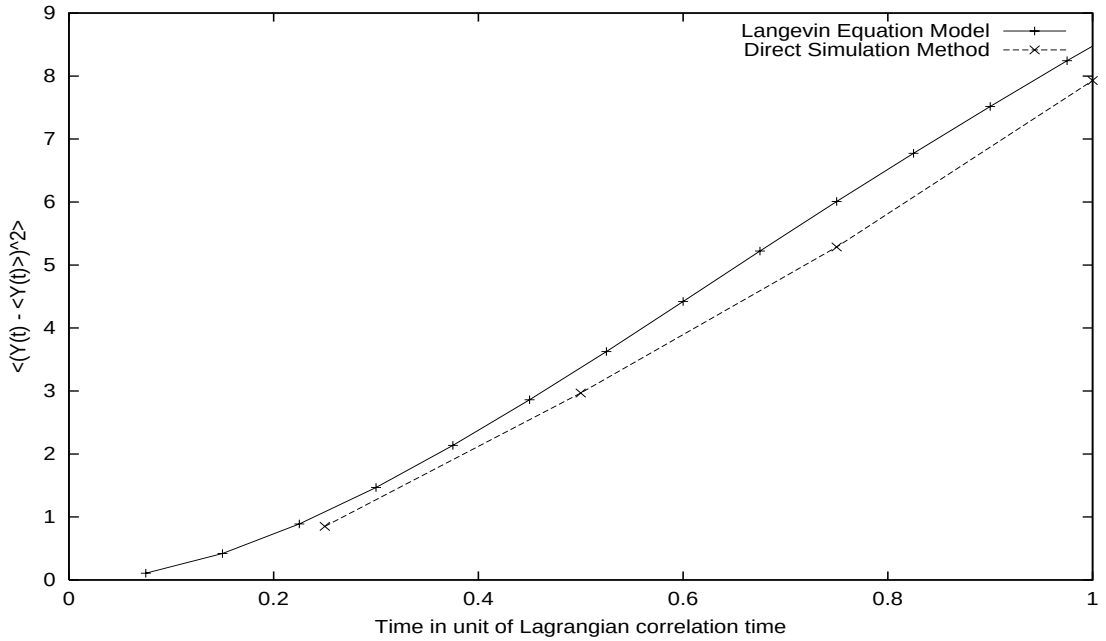

Figure 19: Comparison between Langevin model and DSM of the longitudinal dispersion component for large times.

In the cases mentioned above, we have found that the choice $C_u = 5.$, $u_{\parallel \min} = 0.05$, and $u_{\parallel \max} = 5.$ leads to stable calculations.

The model with tabulated drift coefficients (36) and (37) is quite fast, and with $\alpha = 4.$ it gives stable results well agreed with the time behaviour of the longitudinal and transversal dispersions. Figures 16 and 17 show indeed the result of the comparison for small elapsed time for t up to $0.1\,T_L$, whereas figures 18 and 19 show the results for a time t up to $1\,T_L$. Even if the agreement is not perfect (as for instance in the case of the transverse dispersion at early times), we see that for a first approximation made on the values of the diffusion coefficients $b_\parallel^2$ and $b_\perp^2$, the correct behaviour at early and late times is obtained.

5 Conclusions

A stochastic simulation model based on Langevin type stochastic differential equations, widely used in applications such as contaminant transport of aerosols in the atmosphere, is generalized to the contaminant transport in porous media.

The crucial idea was in the assumption that even in the case of laminar flow in porous media, due to the extremely high heterogeneity, there exists an interval where the acceleration vector behaves like a random diffusion process governed by a stochastic differential equation. The main effort of this paper was in the construction of such a stochastic differential equation consistent with the statistical structure of the Eulerian velocity field. However the extraction of such a statistical information via DSM method applied to the Darcy equation which includes a random hydraulic conductivity was also a hard task.

From the geostatistical models collected in the literature, and by applying a numerical groundwater flow model it has been possible to determine the parameters of the Langevin model in the porous medium. It was important to identify the Eulerian and Lagrangian characteristics of velocity and mainly to find out whether the Lagrangian structure function was presenting a linear behaviour at early times in order to define the drift and diffusion terms of the Langevin model for velocity.

Important part of the work was to compare the new stochastic model to the direct simulation method to see if the Langevin model is able to mimic the transport characteristics of the contaminant transport. We have shown, from a very first approximation of the diffusion coefficients, that this was also possible.

Due to the computational efficiency of the Langevin model in comparison to the direct simulation method and due to its potential generalization to many transport regimes (Fickian or not, for instance), it is believed that these first results are very promising.

Further work should include the generalization to several flow conditions (in an anisotropic log hydraulic conductivity structure, for instance) and should be compared to the common random displacement methods (based on the Fickian hypothesis) used in the hydrogeological literature.

It should be stressed that the advantage of the new stochastic model developed is not only in its numerical efficiency but also in the potential possibility to assimilate the detailed information about the velocity statistics.

References

[1] H. Rodean. Stochastic lagrangian models of turbulent diffusion. *Meteorological Monographs*, 26(48), 1996.

[2] D.J. Thomson. Criteria for the selection of stochastic models of particle trajectories in turbulent flows. *Journal of Fluid Mechanics*, 180:529–556, 1987.

[3] B.L. Sawford. Lagrangian statistical simulation of concentration mean and fluctuation fields. *J. Clim. Appl.*, 24:1152–1166, 1985.

[4] K.K. Sabelfeld. *Monte Carlo Methods in Boundary Value Problems.* Springer-Verlag, New York, 1991.

[5] O.A. Kurbanmuradov and K.K. Sabelfeld. Lagrangian stochastic models for turbulent dispersion in the atmospheric boundary layer. *Boundary-Layer Meteorology*, vol.97 (2000), 2, 191-218.

[6] G. Dagan. *Flow and Transport in Porous Formations.* Springer-Verlag, New York, 1989.

[7] L.W. Gelhar. *Stochastic Subsurface Hydrology.* Prentice Hall, New Jersey, 1993.

[8] A.S. Monin and A.M. Yaglom. *Statistical Fluid Mechanics: Mechanics of Turbulence*, volume 1 and 2. The M.I.T. Press, 1981.

[9] J.H. Cushman. *Dynamics of Fluids in Hierarchical Porous Media.* Academic Press, 1990.

[10] J. Law. A statistical approach to the interstitial heterogeneity of sand reservoirs. *Trans. AIME*, 155:202–222, 1944.

[11] R.A. Freeze. A stochastic-conceptual analysis of one-dimensional groundwater flow in nonuniform homogeneous media. *Water Resources Research*, 11(5):725–741, 1975.

[12] A. Lallemand-Barrès and P. Peaudecerf. Recherche des relations entre la valeur de la dispersivité macroscopique d'un milieu aquifère, ses autres caractéristiques et les conditions de mesure. *Bulletin du B.R.G.M.*, 3(4):277–284, 1978.

[13] Y. Rubin and G. Dagan. Stochastic analysis of boundaries effects on head spatial variability in heterogeneous aquifers : 1. Constant head boundary. *Water Resources Research*, 24(10):1689–1697, 1988.

[14] Y. Rubin and G. Dagan. Stochastic analysis of boundaries effects on head spatial variability in heterogeneous aquifers : 2. Impervious boundary. *Water Resources Research*, 25(4):707–712, 1989.

[15] P. Saladin and V. Fiorotto. Solute transport in highly heterogeneous aquifers. *Water Resources Research*, 34(5):949–961, 1998.

[16] H. Vereecken, G. Lindenmayr, O. Neuendorf, U. Döring, and R. Seidemann. TRACE : A mathematical model for reactive transport in 3D variably saturated porous media. Technical report, Forschungszentrum Jülich, ICG-4, 1994.

[17] O.F. Smidts. *Analyse probabiliste du risque du stockage de déchets radioactifs par la méthode des arbres d'événements continus.* PhD thesis, Université Libre de Bruxelles, Brussels, 1997.

[18] Y. Rubin. Stochastic modeling of macrodispersion in heterogeneous porous media. *Water Resources Research*, 26(1):133–141, 1990.

[19] A. Bellin, P. Saladin, and A. Rinaldo. Simulation of dispersion in heterogeneous porous formation: Statistics, first-order theories, convergence of computations. *Water Resources Resources*, 28(9):2211–2227, 1992.

[20] Y. Rubin and G. Dagan. A note on head and velocity covariances in three-dimensional flow through heterogeneous anisotropic porous media. *Water Resources Research*, 28(5):1463–1470, 1992.

[21] D. Russo. On the velocity covariance and transport modeling in heterogeneous anisotropic porous formations 1. saturated flow. *Water Resources Research*, 31(1):129–137, 1995.

[22] K.-C. Hsu, D. Zhang, and S.P. Neuman. Higher-order effects on flow and transport in randomly heterogeneous porous media. *Water Resources Research*, 32(3):571–582, 1996.

[23] K.-C. Hsu and S.P. Neuman. Second-order expressions for velocity moments in two and three-dimensional statistical anisotropic media. *Water Resources Research*, 33(4):625–637, 1997.

[24] K.-C. Hsu. A general method for obtaining analytical expressions for the first-order velocity covariance in heterogeneous porous media. *Water Resources Research*, 35(7):2273–2277, 1999.